

This work was written as part of one of the author's official duties as an Employee of the United States Government and is therefore a work of the United States Government. In accordance with 17 U.S.C. 105, no copyright protection is available for such works under U.S. Law.

Public Domain Mark 1.0

<https://creativecommons.org/publicdomain/mark/1.0/>

Access to this work was provided by the University of Maryland, Baltimore County (UMBC) ScholarWorks@UMBC digital repository on the Maryland Shared Open Access (MD-SOAR) platform.

**Please provide feedback**

Please support the ScholarWorks@UMBC repository by emailing [scholarworks-group@umbc.edu](mailto:scholarworks-group@umbc.edu) and telling us what having access to this work means to you and why it's important to you. Thank you.

# Geophysical Research Letters

## RESEARCH LETTER

10.1029/2020GL087263

### Key Points:

- Extensive surface melt occurred on the Greenland Ice Sheet on 30–31 July 2019 that included Summit Station
- Unlike the 2012 record event, mass loss in the southwestern ice sheet was not as large, while losses in the northeast were comparable
- The melt patterns were driven by a westward advection of a warm air mass that differs from prior events

### Supporting Information:

- Supporting Information S1

### Correspondence to:

R. I. Cullather,  
richard.cullather@nasa.gov

### Citation:

Cullather, R. I., Andrews, L. C., Croteau, M. J., Digirolamo, N. E., Hall, D. K., Lim, Y.-K., et al. (2020). Anomalous circulation in July 2019 resulting in mass loss on the Greenland Ice Sheet. *Geophysical Research Letters*, 47, e2020GL087263. <https://doi.org/10.1029/2020GL087263>

Received 27 JAN 2020

Accepted 23 AUG 2020

Accepted article online 30 AUG 2020

## Anomalous Circulation in July 2019 Resulting in Mass Loss on the Greenland Ice Sheet

Richard I. Cullather<sup>1,2</sup> , Lauren C. Andrews<sup>1</sup> , Michael J. Croteau<sup>3</sup> , Nicolo E. Digirolamo<sup>4,5</sup>, Dorothy K. Hall<sup>2,4</sup> , Young-Kwon Lim<sup>1,6</sup> , Bryant D. Loomis<sup>3</sup> , Christopher A. Shuman<sup>4,7</sup> , and Sophie M. J. Nowicki<sup>4</sup> 

<sup>1</sup>Global Modeling and Assimilation Office, National Aeronautics and Space Administration, Goddard Space Flight Center, Greenbelt, MD, USA, <sup>2</sup>Earth System Science Interdisciplinary Center, University of Maryland, College Park, MD, USA,

<sup>3</sup>Geodesy and Geophysics Laboratory, National Aeronautics and Space Administration, Goddard Space Flight Center, Greenbelt, MD, USA, <sup>4</sup>Cryospheric Science Laboratory, National Aeronautics and Space Administration, Goddard Space Flight Center, Greenbelt, MD, USA, <sup>5</sup>Science Systems and Applications, Inc., Glenn Dale, MD, USA, <sup>6</sup>Universities Space Research Association, Goddard Earth Sciences Technology and Research, Columbia, MD, USA, <sup>7</sup>Joint Center for Earth Systems Technology, University of Maryland, Baltimore County, Baltimore, MD, USA

**Abstract** Current mass loss on the Greenland Ice Sheet (GrIS) includes a significant contribution from surface runoff. The circumstances associated with melt events are important for understanding the global sea level contribution of the GrIS. In late July 2019, surface melt occurred over 62% of the GrIS, including Summit Station. The general circulation leading to the event is found to be dissimilar to 2012 and other events documented in the 21st century, with warm air associated with remote atmospheric blocking over western Europe eventually transiting west to the GrIS. Gravimetric data indicate that the 2019 summer mass loss was 137 Gt more than the 2004–2010 median, or about 92% of the 2012 record. Mass loss during the event was significant in GrIS northeastern regions in 2019. As compared to 2012, the southwest did not fully participate. Similar circulation patterns have not previously been associated with significant melt.

## 1. Introduction

In recent assessments of global sea level, attention has focused on the contributions of polar ice sheets. Satellite altimetry, gravimetric data, and in situ observation assessments suggest that ice sheet mass loss continues to accelerate (e.g., Meredith et al., 2019). For the Greenland Ice Sheet (GrIS), about half of the current mass loss (50.3%) is attributable to a reduction in surface mass balance, owing to an increase in meltwater runoff (The IMBIE Team, 2019). The processes associated with surface mass loss have been extensively studied, particularly in light of recent melt events (e.g., Cullather et al., 2016; Hanna et al., 2013; Mioduszewski et al., 2016; Trusel et al., 2018; van den Broeke et al., 2017). The summer of 2012 saw widespread melt on the GrIS surface and significant mass loss (Fausto et al., 2016; Hanna et al., 2014; Tedesco et al., 2013), including 11 and 12 July when melt was simultaneously observed on nearly the entire GrIS (Hall et al., 2013). Melt and above-freezing air temperatures were observed at Summit Station (72°N, 38°W, 3,216 m; hereafter “Summit”) on 11 July which, based on glaciological records, had occurred only once previously in the past 800 years (Nghiem et al., 2012). Other melt events have occurred at lower elevations since the turn of the century (Box et al., 2010; Hanna et al., 2008; Steffen et al., 2004; Tedesco et al., 2008). These events exhibit variability in their manner and duration. With rare exceptions for the northern basin (Tedesco et al., 2016), they are persistently focused on the western margins (Graeter et al., 2018), which are located on the windward side of the ice sheet under typical atmospheric circulation patterns (Hanna et al., 2014).

Some examined factors that potentially drive melt events include the role of various surface energy budget components, including (1) enhanced longwave radiative fluxes associated with warm, moist air intrusions and cloudiness (Bennartz et al., 2013; Cullather & Nowicki, 2018; van Tricht et al., 2016); (2) enhanced shortwave flux absorption associated with reduced cloudiness and ice surface darkening due to surface feedbacks, preconditioning through reduced winter or spring snow cover (Dyurgerov & Meier, 1999), or aerosol deposition (Box et al., 2012; Hofer et al., 2017; Tedesco et al., 2011; Thomas et al., 2017); (3) changes in turbulent fluxes (Fausto et al., 2016); (4) the effects of reduced sea ice cover on eastward advecting warm and moist conditions (Liu et al., 2016; Noël et al., 2014; Rennermalm et al., 2009; Stroeve et al., 2017); and

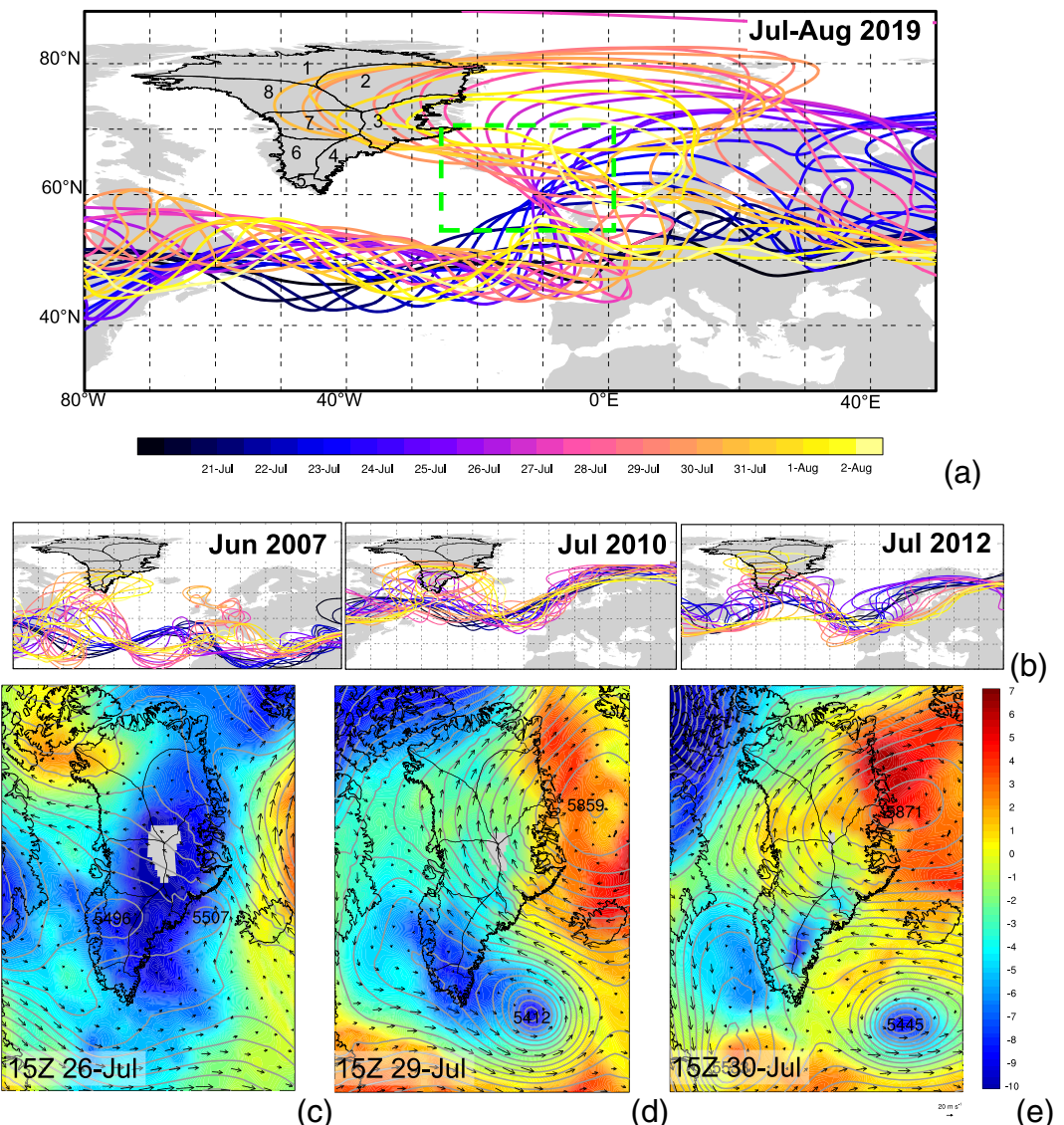


**Figure 1.** (a) The contour line corresponding to a stream function value of  $-5 \cdot 10^7 \text{ m}^2 \text{ s}$  computed from MERRA-2 250 hPa winds, for successive 12-h instances from 20 July through 2 August 2019. The projection highlights zonal and meridional departures. GrIS drainage basins from Zwally et al. (2012) are labeled. A domain used for pattern correlation is indicated with a green dashed line (see text). (b) As in (a) but for melt events (Box et al., 2010; Nghiem et al., 2012) ending 12 June 2007, 21 July 2010, and 12 July 2012. (c–e) 700 hPa temperature field for selected times in 2019, shaded every 0.1°C. Gray shading indicates no data (intersection of 700 hPa level and the surface). The 500 hPa geopotential height field is indicated with contour lines every 20 m. The 250 hPa wind field is indicated with vectors. The reference magnitude is 20 m s<sup>-1</sup>.

(5) various mechanisms of atmospheric circulation, including North Atlantic blocking, circulation trends over the Arctic Ocean (Häkkinen et al., 2014; Hanna et al., 2013; Lim et al., 2016; Tedesco et al., 2016), and extreme moisture transport (Mattingly et al., 2018; Neff, 2018). Local high-pressure blocking has been associated with surface melt events in 2002, 2003, 2007, 2010, and 2012 (Hanna et al., 2008; Nghiem et al., 2012), but prior analysis has suggested that local blocking is an endemic contributor to enhanced surface melt, including lesser events (e.g., Cullather & Nowicki, 2018; Hanna et al., 2016; Lim et al., 2016; Rajewicz & Marshall, 2014). The relation has led to the developed use of the Greenland blocking index (GBI; Hanna et al., 2014).

On 30 and 31 July 2019, widespread surface melt was observed across the GrIS, and above-freezing temperatures were again measured at the NOAA Summit automatic weather station (AWS; Tedesco &

Fettweis, 2019). Here, we employ atmospheric reanalyses (Modern-Era Retrospective analysis for Research and Applications, version 2 [MERRA-2]; Gelaro et al., 2017) and satellite observations from the Moderate-resolution Imaging Spectroradiometer (MODIS; Hall et al., 2018) and the Gravity Recovery and Climate Experiment (GRACE/GRACE-FO) to characterize daily circulation patterns in the week leading to the 2019 event, quantitatively describe the extent and duration of surface melt, examine the amount and spatial distribution of the associated GrIS mass loss, and provide context in relation to prior melt events in the 2003–2018 satellite data record. The analysis reveals that a warm air mass previously associated with a western European heatwave was advected north and westward across the marginal seas of the North Atlantic. Ultimately, this event produced significant melt and mass loss along the northeastern side of the GrIS and enhanced anticyclonic circulation patterns that drove mass loss elsewhere on the ice sheet.

## 2. Atmospheric Conditions

Figure 1a shows the evolving jet stream pattern associated with the melt event in late July and early August 2019. An omega blocking pattern—characterized by a high-amplitude ridge or northward distending area of high pressure in the upper troposphere and surrounded to its east and west by high-amplitude troughs—emerged over western Europe in the early part of the week of 21 July (Figure 1a), producing northward, warm air advection from North Africa. By 24 July, the ridging pattern was centered over western Europe near 9°E, with a lee trough near 30°E and a strengthening windward trough over the central North Atlantic near 28°W. Within this long wave ridging pattern, a minor wave was embedded within the windward trough near the British Isles, which intensified the southerly flow along the western side of the ridge. The blocking pattern resulted in record temperatures in several locations (Graham & Huggett, 2019; Magnusson, 2019). On 25 July, station data (Smith et al., 2011) for Paris-Montsouris, France, reached 42°C while Brussels, Belgium, and Cologne, Germany, exceeded 36°C. On 26 July, reanalyses indicate that the upwind trough of the blocking pattern became negatively tilted (Figure 1a) as the ridge advanced northward to form a closed-circulation anticyclone over Scandinavia. A temperature of 32°C was reached at Bergen, Norway, on 26 July and at Helsinki, Finland, on 27 July. The negative tilt of the trough folded the jet stream into a southeast-to-northwest orientation over the North Atlantic, oriented from the British Isles to eastern Greenland. The surface warm air mass over Europe then followed the westward tilt of the jet stream onto the GrIS, initiating enhanced surface melt on 29 July.

A MODIS data-based analysis of aerosol concentrations (Randles et al., 2017) indicates a large transport from Europe over the North Sea on 26 July, with optical thicknesses of up to 0.1 (Figure S1). The composition is recognized to be largely associated with Saharan dust. Over the subsequent 2 days, the analysis suggests a dispersal over the North Atlantic, with remaining amounts becoming topographically blocked upon nearing Greenland. For the time associated with the melt event, there is insufficient evidence of significant aerosol deposition on the ice sheet.

Rawinsonde data from Scoresbysund (71°N, 22°W, 70 m) for 12 UTC 26 to 29 July indicate an advancing warm layer with temperatures exceeding the prior week's conditions by 5–10°C throughout the troposphere, with an above-freezing layer extending from the surface to 700 hPa (Durre & Yin, 2008; Figures 2c–2e). It may be seen from the profiles that midtropospheric temperatures increased first, with values at Scoresbysund reaching 0°C at 730 hPa on 26 July. The warmest part of the profile is at 839 hPa on 27 July and 814 hPa on 28 July; a near-surface inversion forms after 29 July. A similar downward progression occurred at Danmarkshavn (77°N, 19°W, 11 m) and is consistent with very slow warm air advection. Summit profiles also show a downward progression of temperature increases throughout the troposphere, with an increase of almost 10°C at 500 hPa by 30 July. After 29 July, the Summit profile indicates a near-surface inversion, with the surface pinned near the melting point on 30 July.

## 3. Surface Melt and Mass Loss

Ice surface temperatures (ISTs), indicative of the surface melt/freeze state, were computed from available Terra swath observations from the MODIS for each 24-h period between 25 July and 5 August (Hall et al., 2018). Daily melt extent is determined by applying an IST threshold selected, wherein melt is identified for locations where the IST is greater or equal to the threshold value. The value is based on the accuracy of

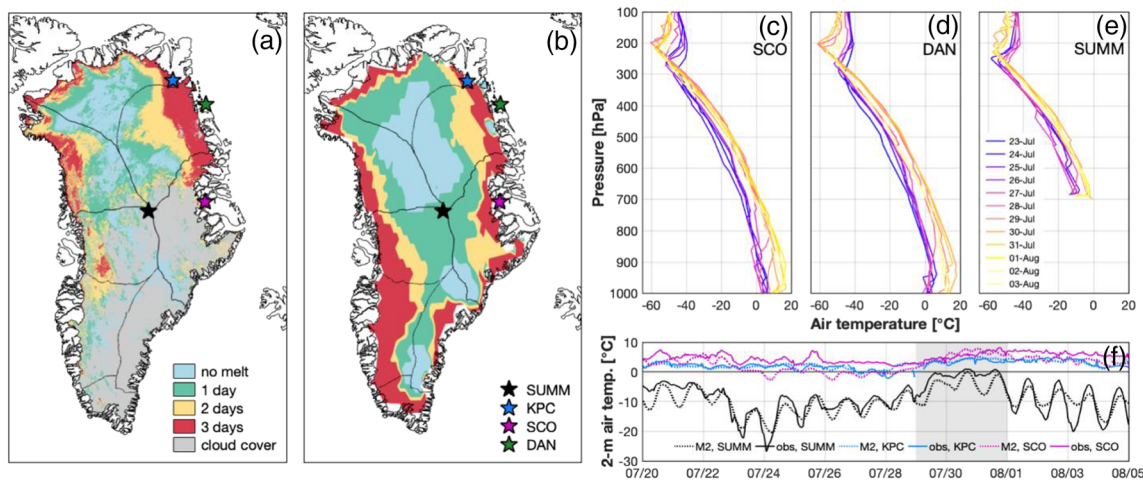


**Figure 2.** The extent of GrIS surface melt over the 3-day period 29 July to 31 July 2019 from (a) MODIS retrieved skin temperature and (b) MERRA-2. Stars indicate the location of meteorological stations Scoresbysund (Ittoqqortoormiit, 71°N, 22°W), Danmarkshavn (77°N, 19°W), and Summit (73°N, 39°W). Temperature sounding profiles are indicated for these stations (c–e) over the period 23 July to 3 August. Hourly surface air temperature time series are shown over the period of the melt event (f).

the product and a long-term comparison with other observations (Adolph et al., 2018). The retrieval is only available for cloud-free conditions (Moeller et al., 2017).

Between 29 July and 1 August, MODIS IST observations indicate that between 21% and 52% of the GrIS experienced surface melt, with a peak observed extent occurring on 1 August as shown in Figure 2a (see also Figure S5). It may be seen from the figure that there is extensive cloud cover just prior and at the onset of the melt event, particularly on 29 and 30 July (covering 22% and 19%, respectively). This restricted the ability of MODIS to detect surface melting across the central and southern GrIS, including Summit. Basins shown in Figure 1 (Zwally et al., 2012) are used to identify regions broadly homogeneous regarding surface slope orientation relative to atmospheric advection. Here, cloud cover was particularly prevalent in Basins 3 and 4. Nevertheless, MODIS IST data indicated substantial melt across the eastern and northern GrIS, with melt extent exceeding 80% of Basin 2 on 30 and 31 July.

Reanalyses may contribute additional information on surface conditions where there is significant cloud cover. MERRA-2 has compared favorably with satellite observations of surface melt (Cullather et al., 2016; Hall et al., 2018; Reeves Eyre & Zeng, 2017) and is used for consistency with the identified general circulation. As noted in Hall et al. (2018), confidence in ice sheet surface properties increases when different data sets are used to produce a similar result. Between 29 July and 1 August, MERRA-2 indicated that between 30% and 62% of the ice sheet experienced surface melting (Figure 2b; see Figure S6). Peak melt extent was observed on 30 July, when 62% of the ice sheet—including Summit—experienced surface skin temperatures at or above 0°C. Surface melt was particularly widespread over central GrIS Basins 3 (89%) and 7 (98%). There was also extensive surface melt on 31 July (61%), though MERRA-2 does not indicate melt at Summit, nor is widespread melt indicated over the central GrIS on this day. Rather, the reanalysis indicates extensive melt in northern Basin 1 (greater than 78%) and in northeastern Basin 2 (48%), as well as large parts of southwestern Basins 5 and 6. MODIS data suggest that the more extensive melt in the northern basins occurred on the prior day, 30 July. Nevertheless, the time-averaged surface melt extent patterns in MODIS and MERRA-2 are in general agreement (Figures 2a and 2b); there are discrepancies in the southern GrIS, where extensive cloud cover during the initial phase of the melt event obscured MODIS retrievals.

Also shown in Figure 2 is the Summit time series of observed air temperatures and corresponding values from reanalyses. Temperatures exceeded 0°C for 11.2 h on 30 July, and again for 5.5 h on 31 July, reaching a maximum value of 1.2°C on the second day. The time series is remarkable and is substantially longer than the historic 2012 event when the melting point was reached for 6.5 h on 1 day (McGrath et al., 2013). Corresponding values from the reanalysis for 2019 indicate some differences in the diurnal cycle but nevertheless approximate the day-to-day variability of the station measurements.

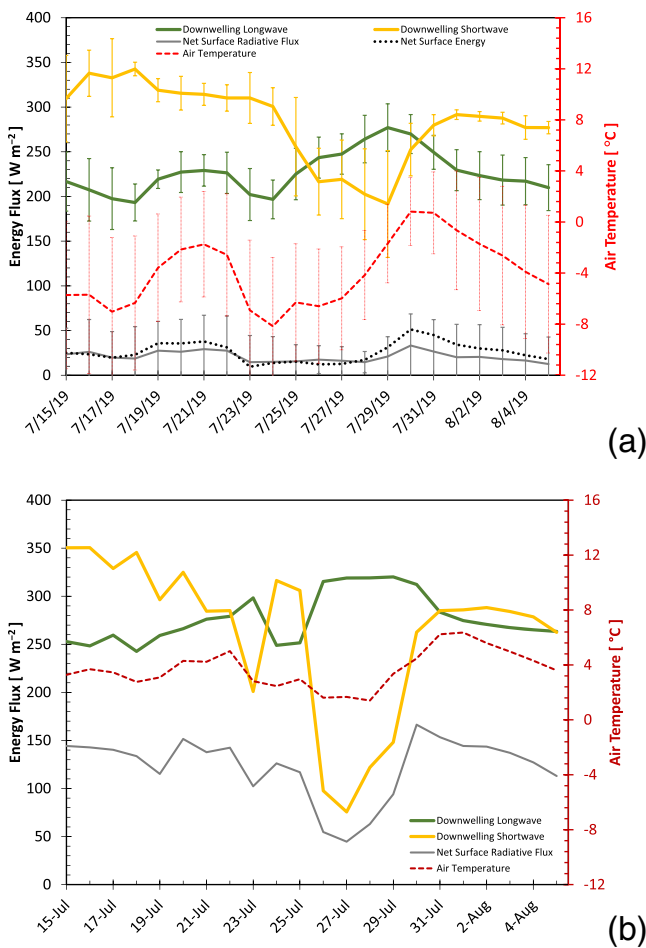


**Figure 3.** Surface energy budget components from (a) MERRA-2, averaged over GrIS Basin 3, and (b) PROMICE AWS station SCO-U (72°N, 27°W, 970 m). Vertical bars indicate the spatial standard deviation of MERRA-2 over Basin 3. Flux values are plotted in  $\text{W m}^{-2}$ , and air temperature is plotted in °C.

significance of the 2019 event. More intriguing is the breakdown of these amounts by basin. In the 2012 event, southwestern Basin 6 accounted for largest fraction, nearly 29% of the total amount. In 2019, Basin 6 only accounted for 19%, while northeastern Basins 2 and 3 contributed 35% of the total. In comparing the 2012 and 2019 events, it is found that the northeastern basins provided similar amounts of runoff, while the southwestern basins provided about 44% less runoff in 2019 as compared with 2012.

Gravimetric solutions from GRACE/GRACE-FO are available at resolutions of 300–500 km and at monthly time scales (Loomis et al., 2020; see Figure S7). Thus, changes over the June to August time period examined here may result from the ambient conditions and are not necessarily directly attributable to the melt event of 30 July to 1 August. The gravimetry observations are also not limited to surface changes but measure total mass variability. Surface melt may impact underlying glacier mass on a delayed time scale, from englacial and subglacial routing and retention (Nienow et al., 2017). These gravimetric observing attributes are realized in comparing total mass loss with reanalysis surface estimates over the melt event, but are nevertheless of interest.

We compute basin-averaged mass loss from GRACE/GRACE-FO from the Univ. Texas at Austin's Center for Space Research (CSR) RL06 Level-2 spherical harmonics solution, using the averaging kernel method (Swenson & Wahr, 2002) and applying GRACE Technical Notes 13 and 14 to restore geocenter motion (Sun et al., 2016) and replace  $C_{20}$  and  $C_{30}$  values (Loomis et al., 2019, 2020). Effects due to glacial isostatic adjustment are removed using the ICE-6G\_D (VM5a) model (Peltier et al., 2018).

An examination of the surface energy budget finds a nuanced time series leading to the melt event. Though reanalysis representations of the GrIS surface energy budget can be problematic (e.g., Cullather et al., 2014), MERRA-2 has reasonably reproduced observed cloud radiative forcing and surface albedo (Wang et al., 2019). The energy budget evolution is also supported by the Scoresbysund AWS (Figure 3). Reanalysis fields indicate that the daily-averaged surface downwelling thermal flux increased markedly over Basin 3 in the eastern GrIS prior to the melt event, while the solar flux decreased. From an average of  $197 \text{ W m}^{-2}$  on 24 July, the longwave flux increased by  $80 \text{ W m}^{-2}$  by 29 July (Figure 3; see Figure S10). From an average of  $301 \text{ W m}^{-2}$  on 24 July, the downwelling shortwave flux was lower by  $109 \text{ W m}^{-2}$  on 29 July. Over the ensuing 2 days, the downwelling longwave flux gradually decreased while the downwelling shortwave flux rapidly increased to pre-event levels. Relative to 29 July, the downwelling longwave flux was  $7 \text{ W m}^{-2}$  lower on 30 July and  $28 \text{ W m}^{-2}$  lower on 31 July, while the shortwave was higher by  $61 \text{ W m}^{-2}$  on 30 July and by  $88 \text{ W m}^{-2}$  on 31 July. During this transitional period, the total downwelling radiative flux, the net surface radiative flux, and the surface air temperature were maxima for the examined period, and ice sheet surface melt became widespread. Turbulent fluxes added an additional  $18 \text{ W m}^{-2}$  during this period, or 41% of the net surface flux. Cloud masking from the MODIS temperature data supports the east-to-west passage of a cloud shield over 26 to 29 July, prior to the arrival of warmest surface temperatures on the eastern GrIS (see Figure S4).

Reanalysis and GRACE/GRACE-FO data are used to characterize mass loss changes associated with this melt event. While MERRA-2 surface runoff has compared favorably with observations (e.g., Smith et al., 2017), the surface representation is of intermediate complexity and has no explicit firn representation (Cullather et al., 2016).

Reanalysis fields suggest that surface runoff increased markedly from 28 July to 2 August, with the largest amount occurring on 31 July of 1.42 Gt. Over this 6-day period, the total runoff was 6.4 Gt. This may be compared with the historic 2012 melt event (Table S1). Over the period 10–15 July of 2012, reanalyses indicate runoff of 7.7 Gt, suggesting the sig-

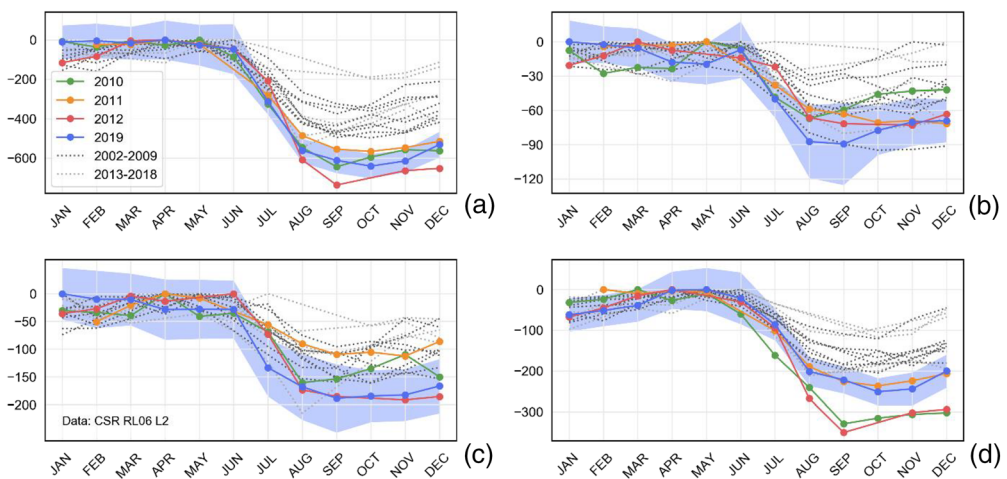


**Figure 4.** Annual cycle of GRACE/GRACE-FO derived mass anomaly relative to each year's maximum value for (a) total GrIS, (b) northern GrIS (Zwally Basin 1), (c) eastern GrIS (Zwally Basins 2 and 3), and (d) southern GrIS (Zwally Basins 4, 5, and 6), in Gt. Select years are indicated, while dotted lines denote all other years in the GRACE/GRACE-FO record. Accumulated errors are shown for 2019; errors for all other years are considered in the analysis but are not overlaid here for clarity. The time series are plotted as anomalies relative to each year's maximum value, which generally occurs in winter and early spring for each of the basins shown.

Figure 4 presents mass loss anomalies relative to each year's maximum value for (a) the total GrIS; (b) northern GrIS, defined as Zwally Basin 1; (c) eastern GrIS, defined as the sum of Basins 2 and 3; and (d) southern GrIS, defined as the sum of Basins 4, 5, and 6. By considering basin clusters, signal leakage errors associated with the limited spatial resolution of monthly GRACE products are mitigated. The reported 2-x1D70E; uncertainties include the solution noise, processing differences, and leakage errors. For the total GrIS, the August minus June monthly values indicate a late summer loss of  $420 \pm 142$  Gt for 2019. This compares with losses of  $459 \pm 140$  and  $443 \pm 125$  Gt for 2012 and 2016, respectively, and a mean loss of  $283 \pm 99$  Gt for the years 2004–2010 (shown in gray). Regionally, the 2019 June-to-August mass losses are  $65 \pm 41$ ,  $114 \pm 79$ , and  $147 \pm 73$  Gt for northern, eastern, and southern GrIS, respectively. For 2012, losses of  $43 \pm 48$ ,  $141 \pm 77$ , and  $194 \pm 54$  Gt are found for the same three regions. We note that the late summer losses in the northern GrIS (Basin 1) are the largest of the GRACE/GRACE-FO record. Combining the northern and eastern regions results in comparable mass losses in 2012 and 2019, while losses in the southern region were a larger contributor in 2012 (42% of the total) than in 2019 (35% of the total). Consistent with reanalysis output for the days encompassing the surface melt, gravimetric data indicate a significant event in 2019 that is somewhat smaller than in July 2012 and with a distinctly different pattern of mass loss.

#### 4. Surface Melt Historical Context

The circulation mechanisms leading to the 2019 melt event contrast with those associated with previous events in the satellite record (e.g., Cullather & Nowicki, 2018; Häkkinen et al., 2014) in several respects. Prior events are largely associated with transient blocking over the North Atlantic, leading to the redirection of subtropical warm air northward over the western GrIS. For example, Figure 1b shows jet stream patterns for several significant melt events in which a high-pressure ridging pattern forms in close proximity to the ice sheet. In the melt event of 12 July 2012, for example, a midlatitude blocking ridge formed near  $35^{\circ}\text{W}$  over several days, eventually extending north to the Denmark Strait and forming a heat dome over the ice sheet that was maintained for an extended period (Nghiem et al., 2012). Such North Atlantic blocking led to a nearly barotropic advection of warm, moist air onto the ice sheet. The 2019 pattern shown here actually coincides with low pressure over the North Atlantic (Figure 1d), although the arrival of the warm air mass eventually resulted in anticyclonic circulation over much of the central and northern regions of the ice sheet. For 2019, the rapid folding of the jet stream resulted in a westward advection of warm air in the middle and upper troposphere that preceded surface warming. The advection is similar to that of a midlatitude warm front, albeit at a greatly slowed rate due to the jet stream folding and planetary wave interaction at higher

latitudes. This baroclinic temperature advection likely resulted in the phased response of surface energy budget components, which differs significantly from previous melt events.

A key aspect of the antecedent circulation is the bending of the jet stream toward the northwest. The streamline configuration of 26 July—oriented from southeast over the British Isles to northwest over the GrIS as contained within the dashed region shown in Figure 1a—was compared with prior summer conditions (June, July, and August [JJA]) in MERRA-2 over the satellite observing era using pattern correlation (see Figure S11). Similar patterns are infrequent but not rare, occurring on average about once per year. An intriguing analogy occurred on 26–28 June 2003 during an extended European heatwave (Black et al., 2004). While the pattern shared characteristics with late July 2019, it did not fully extend westward to the GrIS, and any associated surface melt was largely unremarkable. Limiting factors for this mechanism are the longitudinal range of the jet excursion—which in the 2019 case extended from western Europe all the way to the ice sheet—and access to warm, subtropical air. An additional factor is the duration of the jet folding, which was sustained for several days in 2019 and allowed the warm air mass to traverse onto the ice sheet. Atmospheric heat and moisture transports parallel the jet stream during this event (Figures S2–S4). The values are consistent with an extreme atmospheric moisture transport event (Liu & Barnes, 2015; Mattingly et al., 2018), but again differ in location and orientation to previous melt events examined.

A potential factor in the 2019 event is ice surface preconditioning. Tedesco and Fettweis (2019) note that the 2019 melt season began early, reducing the snowpack. The summer period was characterized by an unusually persistent anticyclone over the GrIS, with a melt event between 11 and 17 June. Passive microwave results of Tedesco and Fettweis (2019) and reanalyses suggest that almost half of the ice sheet experienced melt on 13 June (see Figure S6), potentially leading to decreased surface albedo and snowpack warming, which can result in enhanced feedback mechanisms later in the season.

Persistent high pressure over the ice sheet, as indicated with the GBI, has been associated with reduced cloud cover and enhanced solar radiation, although recent work has also found an association with the northward advection of warm, moist air along the western margins of the ice sheet (Neff et al., 2014). During the late July 2019 event, high pressure likely provided subsidence which allowed warmer air to more rapidly mix downward to the surface. The circulation for this event was confined to the central and northern regions of the GrIS and largely excluded the southwestern margins from the direct influence of advecting warm air (e.g., Figure 1d).

Indices of atmospheric teleconnections are also examined to assess whether the prevailing summertime general circulation was conducive to a melt event. Similar to the GBI, these indices are more associated with central North Atlantic blocking, rather than westward advection indicated for the 2019 event. Studies have shown that the negative phase of the North Atlantic Oscillation (NAO) is more conducive to blocking (e.g., Fettweis et al., 2013; Hanna et al., 2015), while the positive phase of the East Atlantic (EA) pattern—the second principal mode of North Atlantic variability (Trigo et al., 2008)—has also been correlated with enhanced GrIS summer warming (Lim et al., 2016). Principal component-based indices from the NOAA Climate Prediction Center for summer months (JJA) indicate that the NAO was in the negative phase for 2019 and that the index was the seventh lowest value of the 1950–2019 record. The EA index was also strongly positive for JJA, continuing a series of positive values over the last two decades. The JJA average of the GBI was also at a record level (a value of 5,567). In this context, these indices suggest sustained warmer conditions over the summer period which may have preconditioned the ice sheet surface.

## 5. Discussion

A review of the various factors examined in previous melt events highlights unique features of the late July 2019 conditions. The phased time series of surface radiative fluxes shown do not easily comport with prior determinations on the importance of longwave versus shortwave forcing. Rather, an increased net surface energy flux resulted from the interplay of downwelling flux components in the presence of an advancing cloud field. Anomalies in coastal sea ice cover are unlikely to have played a role in the 2019 event. In the vicinity of Scoresbysund, ice extent was only coastally proximal by late July and was similar to recent years in the satellite era (e.g., Fetterer et al., 2017). The ice extent near Fram Strait and in Baffin Bay, which became ice free in mid-July, was also unremarkable in comparison to recent years. While general circulation

indices are consistent with previous melt events, the indices are generally used to identify blocking over or very near the ice sheet, as opposed to the remote blocking that occurred here.

Prior to 2012, surface melt at Summit had occurred once in 800 years (Nghiem et al., 2012) but has now occurred twice in about 7 years. The infrequent nature of melt at Summit and the unusual manner of this event dissuades conclusions regarding trends. Nevertheless, these recent events are consistent with increasing surface melt found elsewhere on the GrIS (The IMBIE Team, 2019).

The large excursion of the jet stream is an intriguing aspect of this event. While some studies have suggested a tendency for low index flow in the presence of a warming climate, such conclusions remain contentious (e.g., Francis & Vavrus, 2012; Gillett & Fyfe, 2013; National Research Council, 2014). In a warming climate, it is possible that the effects of infrequent circulation conditions on the GrIS are simply becoming more acute. It remains to be seen if a wider variety of anomalous circulation patterns may become associated with surface melt under these conditions.

## Data Availability Statement

MERRA-2 (Global Modeling and Assimilation Office, 2015a, 2015b) and MODIS ice surface temperature data were obtained from the Goddard Earth Sciences Data and Information Services Center. Rawinsonde data were obtained from the Integrated Global Rawinsonde Archive, NOAA National Centers for Environmental Information. Climate indices were obtained from the NOAA Climate Prediction Center. Automatic weather station data were obtained from the Programme for Monitoring of the Greenland Ice Sheet (<https://promice.org/PromiceDataPortal/api/download/f24019f7-d586-4465-8181-d4965421e6eb>). Summit temperatures were obtained from the NOAA Earth System Research Laboratory (<https://www.esrl.noaa.gov/gmd/dv/site/index.php?stacode=SUM>) by M. Schnaubelt, Univ. Maryland-Baltimore County. GRACE/GRACE-FO RL06 Level-2 spherical harmonic data (GRACE-FO, 2019) and associated Technical Notes were obtained from Physical Oceanography Distributed Active Archive Center (PO. DAAC) at the Jet Propulsion Lab (<https://podaac.jpl.nasa.gov/>).

## Acknowledgments

The authors thank G.S. Partyka for useful discussions. This work was funded by the NASA Sea Level Change Team and the Modeling, Analysis, and Prediction programs. Michael Croteau's work was also supported by an appointment to the NASA Postdoctoral Program at Goddard Space Flight Center as administered by Universities Space Research Association.

## References

- Adolph, A. C., Albert, M. R., & Hall, D. K. (2018). Near-surface temperature inversion during summer at Summit, Greenland, and its relation to MODIS-derived surface temperatures. *The Cryosphere*, 12(3), 917–920. <https://doi.org/10.5194/tc-12-907-2018>
- Bennartz, R., Shupe, M. D., Turner, D. D., Walden, V. P., Steffen, K., Cox, C. J., et al. (2013). July 2012 Greenland melt extent enhanced by low-level liquid clouds. *Nature*, 496(7443), 83–86. <https://doi.org/10.1038/nature12002>
- Black, E., Blackburn, M., Harrison, G., Hoskins, B., & Methven, J. (2004). Factors contributing to the summer 2003 European heatwave. *Weather*, 59(8), 217–223. <https://doi.org/10.1256/wea.74.04>
- Box, J. E., Cappelen, J., Decker, D., Fettweis, X., Mote, T., Tedesco, M., & van de Wal, R. S. W. (2010). Greenland. In J. Richter-Menge & J. E. Overland (Eds.), *Arctic report card: Update for 2010* (pp. 55–64). Washington, DC: US Department of Commerce. <https://doi.org/10.7916/D8XW4JQX>
- Box, J. E., Fettweis, X., Stroeve, J. C., Tedesco, M., Hall, D. K., & Steffen, K. (2012). Greenland ice sheet albedo feedback. Thermodynamics and atmospheric drivers. *The Cryosphere*, 6(4), 821–839. <https://doi.org/10.5194/tc-6-821-2012>
- Cullather, R. I., & Nowicki, S. M. J. (2018). Greenland Ice Sheet surface melt and its relation to daily atmospheric conditions. *Journal of Climate*, 31(5), 1897–1919. <https://doi.org/10.1175/JCLI-D-17-0447.1>
- Cullather, R. I., Nowicki, S. M. J., Zhao, B., & Koenig, L. S. (2016). A characterization of Greenland Ice Sheet surface melt and runoff in contemporary reanalyses and a regional climate model. *Frontiers in Earth Science*, 4, 10. <https://doi.org/10.3389/feart.2016.00010>
- Cullather, R. I., Nowicki, S. M. J., Zhao, B., & Suarez, M. J. (2014). Evaluation of the surface representation of the Greenland Ice Sheet in a general circulation model. *Journal of Climate*, 27(13), 4835–4856. <https://doi.org/10.1175/JCLI-D-13-00635.1>
- Durre, I., & Yin, X. (2008). Enhanced radiosonde data for studies of vertical structure. *Bulletin of the American Meteorological Society*, 89(9), 1257–1262. <https://doi.org/10.1175/2008BAMS2603.1>
- Dyurgerov, M. B., & Meier, M. F. (1999). Analysis of winter and summer glacier mass balances. *Geografiska Annaler Series A*, 81(4), 541–554. <https://doi.org/10.1111/j.0435-3676.1999.00082.x>
- Fausto, R. S., van As, D., Box, J. E., Colgan, W., Langen, P. L., & Mottram, R. H. (2016). The implication of nonradiative energy fluxes dominating Greenland Ice Sheet exceptional ablation area surface melt in 2012. *Geophysical Research Letters*, 43, 2649–2658. <https://doi.org/10.1002/2016GL067720>
- Fetterer, F., Knowles, K., Meier, W. N., Savoie, M., & Windnagel, A. K. (2017). *Sea ice index, version 3*. Boulder, Colorado USA: NSIDC: National Snow and Ice Data Center. <https://doi.org/10.7265/N5K072F8>
- Fettweis, X., Hanna, E., Lang, C., Bellefamme, A., Erpicum, M., & Gallée, H. (2013). Important role of the mid-tropospheric atmospheric circulation in the recent surface melt increase over the Greenland Ice Sheet. *The Cryosphere*, 7(1), 241–248. <https://doi.org/10.5194/tc-7-241-2013>
- Francis, J. A., & Vavrus, S. J. (2012). Evidence linking Arctic amplification to extreme weather in mid-latitudes. *Geophysical Research Letters*, 39, L06801. <https://doi.org/10.1029/2012GL051000>
- Gelaro, R., McCarty, W., Suárez, M. J., Todling, R., Molod, A., Takacs, L., et al. (2017). The Modern-Era Retrospective Analysis for Research and Applications, version 2 (MERRA-2). *Journal of Climate*, 30(13), 5419–5454. <https://doi.org/10.1175/JCLI-D-16-0758.1>

- Gillett, N. P., & Fyfe, J. C. (2013). Annular mode changes in the CMIP5 simulations. *Geophysical Research Letters*, 40, 1189–1193. <https://doi.org/10.1002/grl.50249>
- Global Modeling and Assimilation Office (2015a). MERRA-2 tavg1\_2d\_slv\_Nx: 2d, 1-Hourly, TIme-Averaged, Single-Level, Assimilation, Single-Level Diagnostics, Ver. 5.12.4. GES DISC, MD, USA. <https://doi.org/10.5067/VJAFPL1CSIV>
- Global Modeling and Assimilation Office (2015b). MERRA-2 tavg1\_2d\_rad\_Nx: 2d, 1-Hourly, Time-Averaged, Single-Level, Assimilation, Radiation Diagnostics, Ver. 5.12.4. GES DISC, MD, USA. <https://doi.org/10.5067/Q9QMY5PBNV1T>
- GRACE-FO (2019). GRACE-FO Level-2 Monthly Geopotential Spherical Harmonics CSR Release 6.0 (RL06). Ver. 6. PO.DAAC, CA, USA. Dataset accessed 2019-11-25 at <https://doi.org/10.5067/GFL20-MC060>
- Graeter, K. A., Osterberg, E. C., Ferris, D. G., Hawley, R. L., Marshall, H. P., Lewis, G., et al. (2018). Ice core records of West Greenland melt and climate forcing. *Geophysical Research Letters*, 45, 3164–3172. <https://doi.org/10.1002/2017GL076641>
- Graham, E., & Huggett, G. (Eds) (2019). New UK maximum air temperature record. *Weather*, 74(9), 294. <https://doi.org/10.1002/wea.3347>
- Häkkinen, S., Hall, D. K., Shuman, C. A., Worthen, D. L., & DiGirolamo, N. E. (2014). Greenland ice sheet melt from MODIS and associated atmospheric variability. *Geophysical Research Letters*, 41, 1600–1607. <https://doi.org/10.1002/2013GL059185>
- Hall, D. K., Comiso, J. C., DiGirolamo, N. E., Shuman, C. A., Box, J. E., & Koenig, L. S. (2013). Variability in the surface temperature and melt extent of the Greenland Ice Sheet from MODIS. *Geophysical Research Letters*, 40, 2114–2120. <https://doi.org/10.1002/grl.50240>
- Hall, D. K., Cullather, R. I., DiGirolamo, N. E., Comiso, J. C., Medley, B. C., & Nowicki, S. M. (2018). A multilayer surface temperature, surface albedo and water vapor product of Greenland from MODIS. *Remote Sensing*, 10, 555. <https://doi.org/10.3390/rs10040555>
- Hanna, E., Cropper, T. E., Hall, R. J., & Cappelen, J. (2016). Greenland blocking index 1851–2015. A regional climate change signal. *International Journal of Climatology*, 36(15), 4847–4861. <https://doi.org/10.1002/joc.4673>
- Hanna, E., Cropper, T. E., Jones, P. D., Scaife, A. A., & Allan, R. (2015). Recent seasonal asymmetric changes in the NAO (a marked summer decline and increased winter variability) and associated changes in the AO and Greenland blocking index. *International Journal of Climatology*, 35(9), 2540–2554. <https://doi.org/10.1002/joc.4157>
- Hanna, E., Fettweis, X., Mernild, S. H., Cappelen, J., Rønne, M. H., Shuman, C. A., et al. (2014). Atmospheric and oceanic climate forcing of the exceptional Greenland Ice Sheet surface melt in summer 2012. *International Journal of Climatology*, 34(4), 1022–1037. <https://doi.org/10.1002/joc.3743>
- Hanna, E., Huybrechts, P., Steffen, K., Cappelen, J., Huff, R., Shuman, C., et al. (2008). Increased runoff from melt from the Greenland Ice Sheet. A response to global warming. *Journal of Climate*, 21(2), 331–341. <https://doi.org/10.1175/2007JCLI1964.1>
- Hanna, E., Jones, J. M., Cappelen, J., Mernild, S. H., Wood, L., Steffen, K., & Huybrechts, P. (2013). The influence of North Atlantic atmospheric and oceanic forcing effects on 1900–2010 Greenland summer climate and ice melt/runoff. *International Journal of Climatology*, 33(4), 862–880. <https://doi.org/10.1002/joc.3475>
- Hofer, S., Tedstone, A. J., Fettweis, X., & Bamber, J. L. (2017). Decreasing cloud cover drives the recent mass loss on the Greenland Ice Sheet. *Science Advances*, 3, e1700584. <https://doi.org/10.1126/sciadv.1700584>
- Lim, Y.-K., Schubert, S. D., Nowicki, S. M. J., Lee, J. N., Molod, A. M., Cullather, R. I., et al. (2016). Atmospheric summer teleconnections and Greenland Ice Sheet surface mass variations. Insights from MERRA-2. *Environmental Research Letters*, 11, 024002. <https://doi.org/10.1088/1748-9326/11/2/024002>
- Liu, C., & Barnes, E. A. (2015). Extreme moisture transport into the Arctic linked to Rossby wave breaking. *Journal of Geophysical Research: Atmospheres*, 120, 3774–3788. <https://doi.org/10.1002/2014JD022796>
- Liu, J. P., Chen, Z. Q., Francis, J., Song, M. R., Mote, T., & Hu, Y. Y. (2016). Has Arctic Sea ice loss contributed to increased surface melting of the Greenland Ice Sheet? *Journal of Climate*, 29(9), 3373–3386. <https://doi.org/10.1175/JCLI-D-15-0391.1>
- Loomis, B. D., Rachlin, K. E., & Luthcke, S. B. (2019). Improved Earth oblateness rate reveals increased ice sheet losses and mass-driven sea level rise. *Geophysical Research Letters*, 46, 6910–6917. <https://doi.org/10.1029/2019GL082929>
- Loomis, B. D., Rachlin, K. E., Wiese, D. N., Landerer, F. W., & Luthcke, S. B. (2020). Replacing GRACE/GRACE-FO C30 with satellite laser ranging. Impacts on Antarctic Ice Sheet mass change. *Geophysical Research Letters*, 47, e2019GL085488. <https://doi.org/10.1029/2019GL085488>
- Magnusson, L. (2019). The 2019 western European heatwaves. *ECMWF Newsletter*, 161, 2–3. Reading, United Kingdom: European Centre for Medium Range Weather Forecasts.
- Mattingly, K. S., Mote, T. L., & Fettweis, X. (2018). Atmospheric river impacts on Greenland Ice Sheet surface mass balance. *Journal of Geophysical Research: Atmospheres*, 123, 8538–8560. <https://doi.org/10.1029/2018JD028714>
- McGrath, D., Colgan, W., Bayou, N., Muto, A., & Steffen, K. (2013). Recent warming at Summit, Greenland. Global context and implications. *Geophysical Research Letters*, 40, 2091–2096. <https://doi.org/10.1002/grl.50456>
- Meredith, M., Sommerkorn, M., Cassotta, S., DerkSEN, C., Ekaykin, A., Hollowed, A., et al. (2019). Polar regions. In H.-O. Pörtner, D. C. Roberts, V. Masson-Delmotte, P. Zhai, M. Tignor, E. Poloczanska, K. Mintenbeck, A. Alegría, M. Nicolai, A. Okem, J. Petzold, B. Rama, & N. M. Weyer (Eds.), *IPCC special report on the ocean and cryosphere in a changing climate* (pp. 203–320). Geneva, Switzerland: IPCC Intergovernmental Panel on Climate Change.
- Mioduszewski, J. R., Rennermalm, A. K., Hammann, A., Tedesco, M., Noble, E. U., Stroeve, J. C., & Mote, T. L. (2016). Atmospheric drivers of Greenland surface melt revealed by self-organizing maps. *Journal of Geophysical Research: Atmospheres*, 121, 5095–5114. <https://doi.org/10.1002/2015JD024550>
- Moeller, C., Frey, R., Borbas, E., Menzel, W. P., Wilson, T., Wu, A., & Geng, X. (2017). Improvements to Terra MODIS L1B, L2, and L3 science products through using crosstalk corrected L1B radiances. *Proceedings SPIE 10402 Earth Observing Systems, XXII*, 1040200. <https://doi.org/10.1117/12.2274340>
- National Research Council (2014). *Linkages between Arctic warming and mid-latitude weather patterns: Summary of a workshop* (p. 85). Washington, DC: The National Academies Press. <https://doi.org/10.17226/18727>
- Neff, W. (2018). Atmospheric rivers melt Greenland. *Nature Climate Change*, 8(10), 857–858. <https://doi.org/10.1038/s41558-018-0297-4>
- Neff, W., Compo, G. P., Ralph, F. M., & Shupe, M. D. (2014). Continental heat anomalies and the extreme melting of the Greenland ice surface in 2012 and 1889. *Journal of Geophysical Research: Atmospheres*, 119, 6520–6536. <https://doi.org/10.1002/2014JD021470>
- Nghiem, S. V., Hall, D. K., Mote, T. L., Tedesco, M., Albert, M. R., Keegan, K., et al. (2012). The extreme melt across the Greenland Ice Sheet in 2012. *Geophysical Research Letters*, 39, L20502. <https://doi.org/10.1029/2012GL053611>
- Nienow, P. W., Sole, A. J., Slater, D. A., & Cowton, T. R. (2017). Recent advances in our understanding of the role of meltwater in the Greenland Ice Sheet system. *Current Climate Change Reports*, 3(4), 330–344. <https://doi.org/10.1007/s40641-017-0083-9>
- Noël, B., Fettweis, X., van de Berg, W. J., van den Broeke, M. R., & Erpicum, M. (2014). Sensitivity of Greenland Ice Sheet surface mass balance to perturbations in sea surface temperature and sea ice cover. A study with the regional climate model MAR. *The Cryosphere*, 8(5), 1871–1883. <https://doi.org/10.5194/tc-8-1871-2014>

- Peltier, W. R., Argus, D. F., & Drummond, R. (2018). Comment on “an assessment of the ICE-6G\_C (VM5a) glacial isostatic adjustment model” by Purcell et al. *Journal of Geophysical Research: Solid Earth*, 123, 2019–2018. <https://doi.org/10.1002/2016JB013844>
- Rajewicz, J., & Marshall, S. J. (2014). Variability and trends in anticyclonic circulation over the Greenland Ice Sheet, 1948–2013. *Geophysical Research Letters*, 41, 2842–2850. <https://doi.org/10.1002/2014GL059255>
- Randles, C.A., da Silva, A.M., Buchard, V., Darmenov, A., Colarco, P.R., Aquila, V., et al. (2017). The MERRA-2 aerosol assimilation. *NASA Technical Reports*, 45, 140. Retrieved from <https://gmao.gsfc.nasa.gov/pubs/docs/Randles887.pdf>
- Reeves Eyre, J. E., & Zeng, X. (2017). Evaluation of Greenland near surface air temperature datasets. *The Cryosphere*, 11(4), 1591–1605. <https://doi.org/10.5194/tc-11-1591-2017>
- Rennermalm, A. K., Smith, L. C., Stroeve, J. C., & Chu, V. W. (2009). Does sea ice influence Greenland ice sheet surface-melt? *Environmental Research Letters*, 4, 024011. <https://doi.org/10.1088/1748-9326/4/2/024011>
- Smith, A., Lott, N., & Vose, R. (2011). The integrated surface database: Recent developments and partnerships. *Bulletin American Meteorology Society*, 92(6), 704–708. <https://doi.org/10.1175/2011BAMS3015.1>
- Smith, L. C., Yang, K., Pitcher, L. H., Overstreet, B. T., Chu, V. W., Rennermalm, Å. K., et al. (2017). Direct measurements of meltwater runoff on the Greenland Ice Sheet surface. *Proceedings of the National Academy of Sciences*, 114(50), E10622–E10631. <https://doi.org/10.1073/pnas.1707743114>
- Steffen, K., Nghiem, S. V., Huff, R., & Neumann, G. (2004). The melt anomaly of 2002 on the Greenland Ice Sheet from active and passive microwave satellite observations. *Geophysical Research Letters*, 31, L20402. <https://doi.org/10.1029/2004GL020444>
- Stroeve, J. C., Mioduszewski, J. R., Rennermalm, A., Boisvert, L. N., Tedesco, M., & Robinson, D. (2017). Investigating the local-scale influence of sea ice on Greenland surface melt. *The Cryosphere*, 11(5), 2363–2381. <https://doi.org/10.5194/tc-11-2363-2017>
- Sun, Y., Riva, R., & Ditmar, P. (2016). Optimizing estimates of annual variations and trends in geocenter motion and J2 from a combination of GRACE data and geophysical models. *Journal of Geophysical Research: Solid Earth*, 121, 8352–8370. <https://doi.org/10.1002/2016JB013073>
- Swenson, S., & Wahr, J. (2002). Methods for inferring regional surface-mass anomalies from Gravity Recovery and Climate Experiment (GRACE) measurements of time-variable gravity. *Journal of Geophysical Research*, 107(B9), 2193. <https://doi.org/10.1029/2001JB000576>
- Tedesco, M., & Fettweis, X. (2019). Unprecedented atmospheric conditions (1948–2019) drive the 2019 exceptional melting season over the Greenland Ice Sheet. *The Cryosphere Discussions*, 14, 1209–1223. <https://doi.org/10.5194/tc-2019-254>
- Tedesco, M., Fettweis, X., Mote, T., Wahr, J., Alexander, P., Box, J. E., & Wouters, B. (2013). Evidence and analysis of 2012 Greenland records from spaceborne observations, a regional climate model and reanalysis data. *The Cryosphere*, 7(2), 615–630. <https://doi.org/10.5194/tc-7-615-2013>
- Tedesco, M., Fettweis, X., van den Broeke, M. R., van de Wal, R. S. W., Smeets, C. J. P. P., van de Berg, W. J., et al. (2011). The role of albedo and accumulation in the 2010 melting record in Greenland. *Environmental Research Letters*, 6, 014005. <https://doi.org/10.1088/1748-9326/6/1/014005>
- Tedesco, M., Mote, T., Fettweis, X., Hanna, E., Jeyaratnam, J., Booth, J. F., et al. (2016). Arctic cut-off high drives the poleward shift of a new Greenland melting record. *Nature Communications*, 7, 11723. <https://doi.org/10.1038/ncomms11723>
- Tedesco, M., Serreze, M., & Fettweis, X. (2008). Diagnosing the extreme surface melt event over southwestern Greenland in 2007. *The Cryosphere*, 2(2), 159–166. <https://doi.org/10.5194/tc-2-159-2008>
- The IMBIE Team (2019). Mass balance of the Greenland Ice Sheet from 1992 to 2018. *Nature*, 579(7798), 233–239. <https://doi.org/10.1038/s41586-019-1855-2>
- Thomas, J. L., Polashenski, C. M., Soja, A. J., Marelle, L., Casey, K. A., Choi, H. D., et al. (2017). Quantifying black carbon deposition over the Greenland Ice Sheet from forest fires in Canada. *Geophysical Research Letters*, 44, 7965–7974. <https://doi.org/10.1002/2017GL073701>
- Trigo, R. M., Valente, M. A., Trigo, I. F., Miranda, P. M. A., Ramos, A. M., Paredes, D., & García-Herrera, R. (2008). The impact of North Atlantic wind and cyclone trends on European precipitation and significant wave height in the Atlantic. *Annals New York Academy of Sciences*, 1146(1), 212–234. <https://doi.org/10.1196/annals.1446.014>
- Trusel, L. D., Das, S. B., Osman, M. B., Evans, M. J., Smith, B. E., Fettweis, X., et al. (2018). Nonlinear rise in Greenland runoff in response to post-industrial Arctic warming. *Nature*, 564(7734), 104–108. <https://doi.org/10.1038/s41586-018-0752-4>
- van den Broeke, M. R., Box, J., Fettweis, X., Hanna, E., Noël, B., Tedesco, M., et al. (2017). Greenland Ice Sheet surface mass loss: Recent developments in observation and modeling. *Current Climate Change Report*, 3(4), 345–356. <https://doi.org/10.1007/s40641-017-0084-8>
- van Tricht, K., Lhermitte, S., Lenaerts, J. T. M., Gorodetskaya, I. V., L'Ecuyer, T. S., Noël, B., et al. (2016). Clouds enhance Greenland Ice Sheet meltwater runoff. *Nature Communications*, 7, 10266. <https://doi.org/10.1038/ncomms10266>
- Wang, W., Zender, C. S., van As, D., & Miller, N. B. (2019). Spatial distribution of melt season cloud radiative effects over Greenland: Evaluating satellite observations, reanalyses, and model simulations against in situ measurements. *Journal of Geophysical Research: Atmospheres*, 124, 57–71. <https://doi.org/10.1029/2018JD028919>
- Zwally, H. J., Giovinetto, M. B., Beckley, M. A., & Saba, J. L. (2012). Data from: Antarctic and Greenland drainage systems. NASA GSFC Cryospheric Sciences Laboratory. Retrieved from [http://icesat4.gsfc.nasa.gov/cryo\\_data/ant\\_grn\\_drainage\\_systems.php](http://icesat4.gsfc.nasa.gov/cryo_data/ant_grn_drainage_systems.php)



*Geophysical Research Letters*

Supporting Information for

## Anomalous circulation in July 2019 resulting in mass loss on the Greenland Ice Sheet

Richard I. Cullather<sup>1,2</sup>, Lauren C. Andrews<sup>1</sup>, Michael J. Croteau<sup>3</sup>, Nicolo E. Digirolamo<sup>4,5</sup>, Dorothy K. Hall<sup>2,4</sup>, Young-Kwon Lim<sup>1,6</sup>, Bryant D. Loomis<sup>3</sup>, Christopher A. Shuman<sup>4,7</sup>, and Sophie M.J. Nowicki<sup>4</sup>

<sup>1</sup>Global Modeling and Assimilation Office, National Aeronautics and Space Administration, Goddard Space Flight Center, Greenbelt, Maryland, USA.

<sup>2</sup>Earth System Science Interdisciplinary Center, University of Maryland, College Park, Maryland, USA.

<sup>3</sup>Geodesy and Geophysics Laboratory, National Aeronautics and Space Administration, Goddard Space Flight Center, Greenbelt, Maryland, USA.

<sup>4</sup>Cryospheric Science Laboratory, National Aeronautics and Space Administration, Goddard Space Flight Center, Greenbelt, Maryland, USA.

<sup>5</sup>Science Systems and Applications, Inc., Glenn Dale, Maryland, USA.

<sup>6</sup>Universities Space Research Association, Goddard Earth Sciences Technology and Research, Columbia, Maryland, USA.

<sup>7</sup>University of Maryland, Baltimore County, Baltimore, Maryland, USA

### Contents of this file

Table S1

Figures S1 to S11

### Introduction

This supplemental section provides additional information on the processes examined in this study. Specifically, Table 1 and Figures S1-S11 which could not be included in the main body of the text due to length restrictions are provided, as they may give additional context and background for the reader. Table 1 provides a comparison of the 2012 and 2019 melt events in reanalysis values for runoff. Figures S1-S4 show spatial patterns associated with transport onto the ice sheet. Figures S5-S7 indicate the pattern and variation of surface melt and runoff. Figures S8-S10 are related to the ice sheet surface energy budget. Finally, Fig. S11 indicates the past frequency of occurrence for the circulation pattern associated with the 2019 event.

**Table S1.** Accumulated MERRA-2 surface runoff for events in July 2012 and July-August 2019, in Gt.

	GrIS Basin								Total
	1	2	3	4	5	6	7	8	
10-July to 15-Jul 2012	0.663	0.749	1.049	0.674	0.547	2.199	0.666	1.148	7.695
28-Jul to 02-Aug 2019	0.729	0.876	1.320	0.535	0.377	1.226	0.517	0.782	6.361

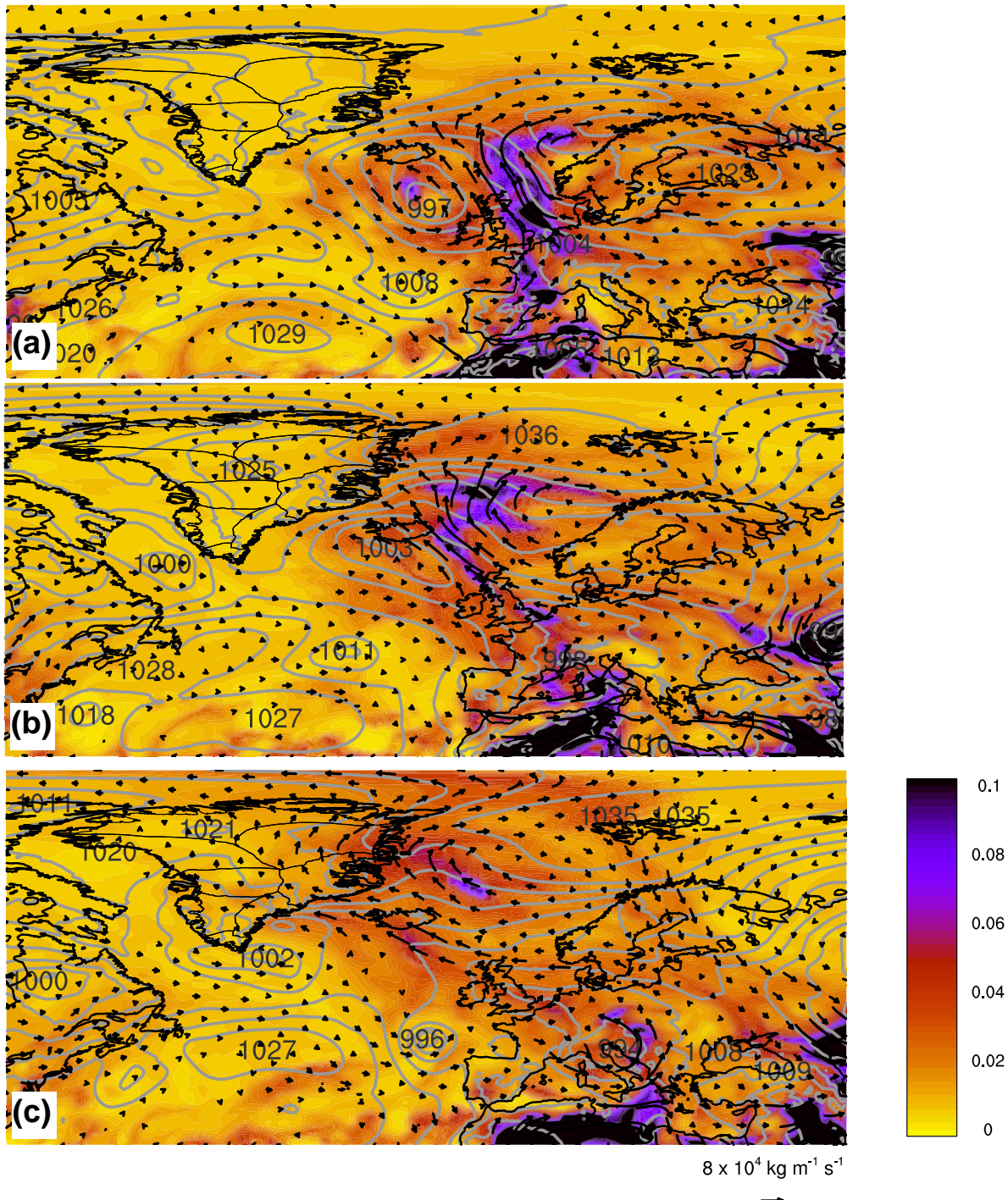


**Figure S1.** MERRA-2 GOCART analyzed dust scattering aerosol optical thickness (550 nm) for 15Z on (a) 26-July, (b), 27-July, and (c) 28-July, shaded every 0.002 (non-dimensional). Vectors indicate the analyzed dust column-integrated mass transport, in  $10^4 \text{ kg m}^{-1} \text{s}^{-1}$ . Sea level pressure is contoured every 4 hPa, with local maxima indicated.

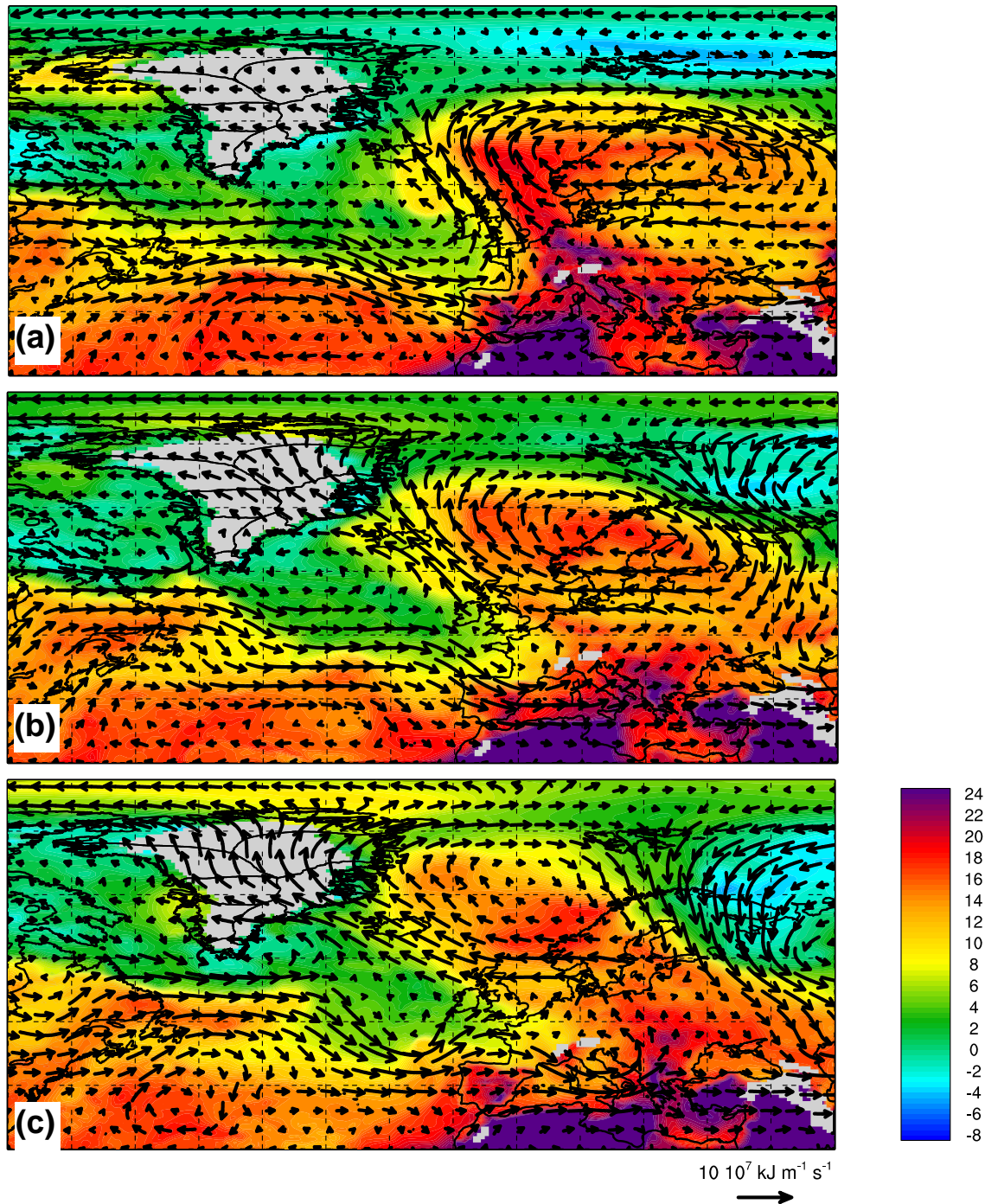


**Figure S2.** MERRA-2 daily-averaged 850 hPa temperatures and total energy transport (the sum of enthalpy, potential, kinetic, and latent fluxes) for (a) 26-July, (b), 27-July, and (c) 28-July. Temperatures are shaded every 0.5 K. Vectors indicate the vertically-integrated energy transport, in  $10^7 \text{ kJ m}^{-1} \text{s}^{-1}$ .

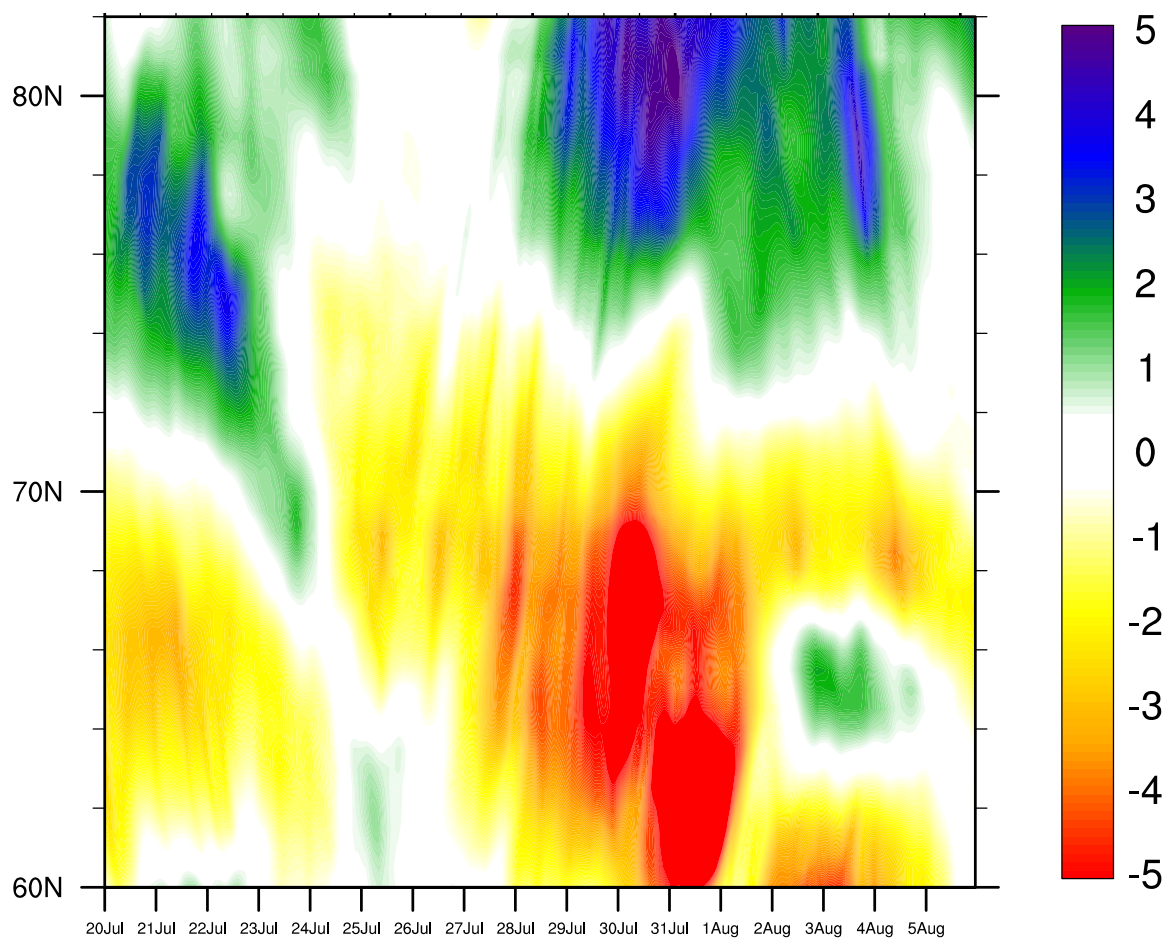


**Figure S3.** MERRA-2 vertically integrated zonal energy transport across  $24^{\circ}\text{W}$  – along the eastern Greenland coastline – for the period 20-July to 5-August, in  $10^7 \text{ kJ m}^{-1} \text{ s}^{-1}$ . Positive values indicate eastward transport.

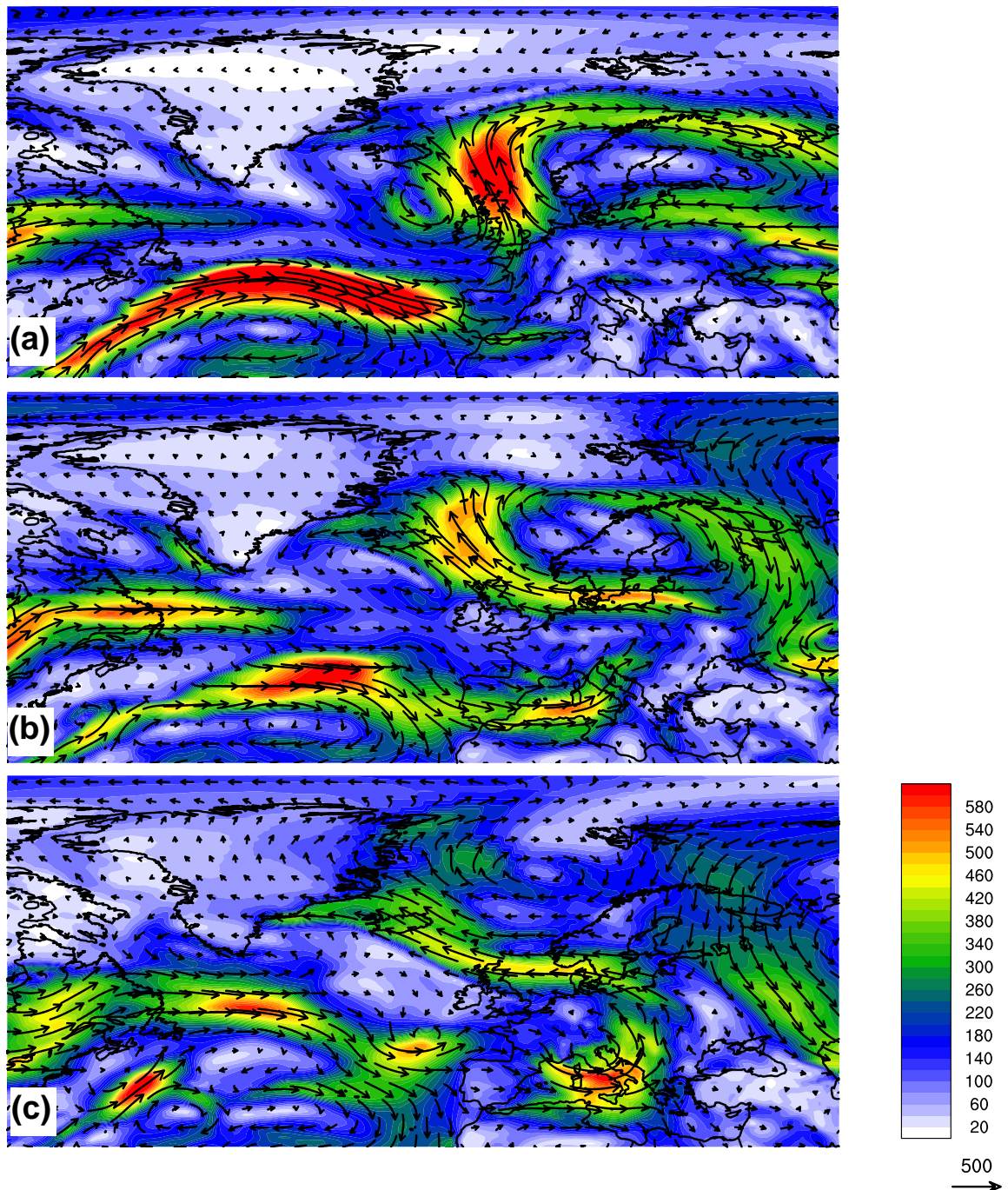


**Figure S4.** MERRA-2 daily-averaged integrated water vapor transport vectors and magnitude for (a) 26-July, (b), 27-July, and (c) 28-July. Vector magnitudes are shaded every  $20 \text{ kg m}^{-1} \text{s}^{-1}$ .

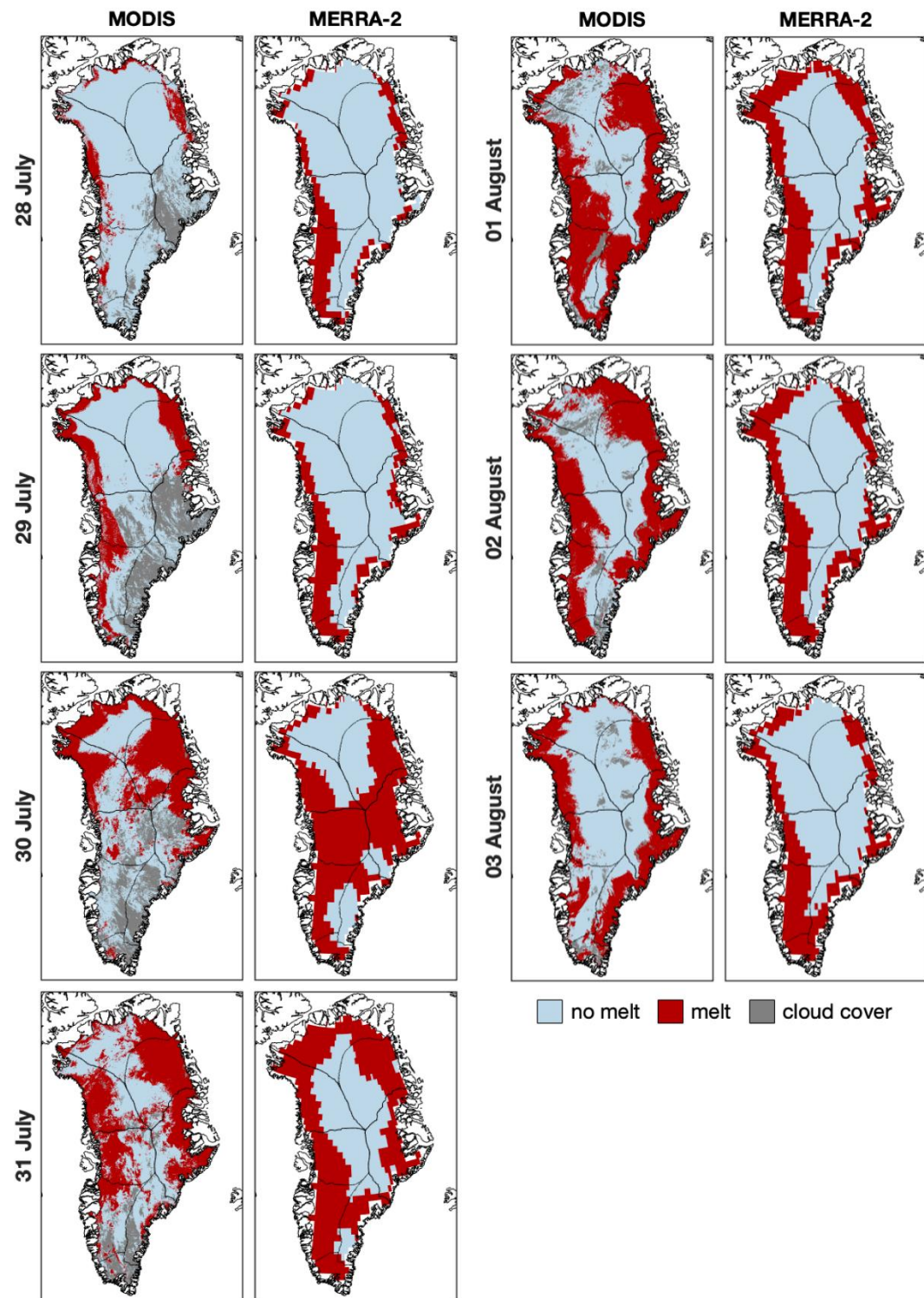


**Figure S5.** Daily melt extent over the July 2019 melt event from MODIS IST (left column) and MERRA-2 (right column). Frozen (blue) and melting (red) areas are indicated. Areas masked by cloud cover are indicated in grey.

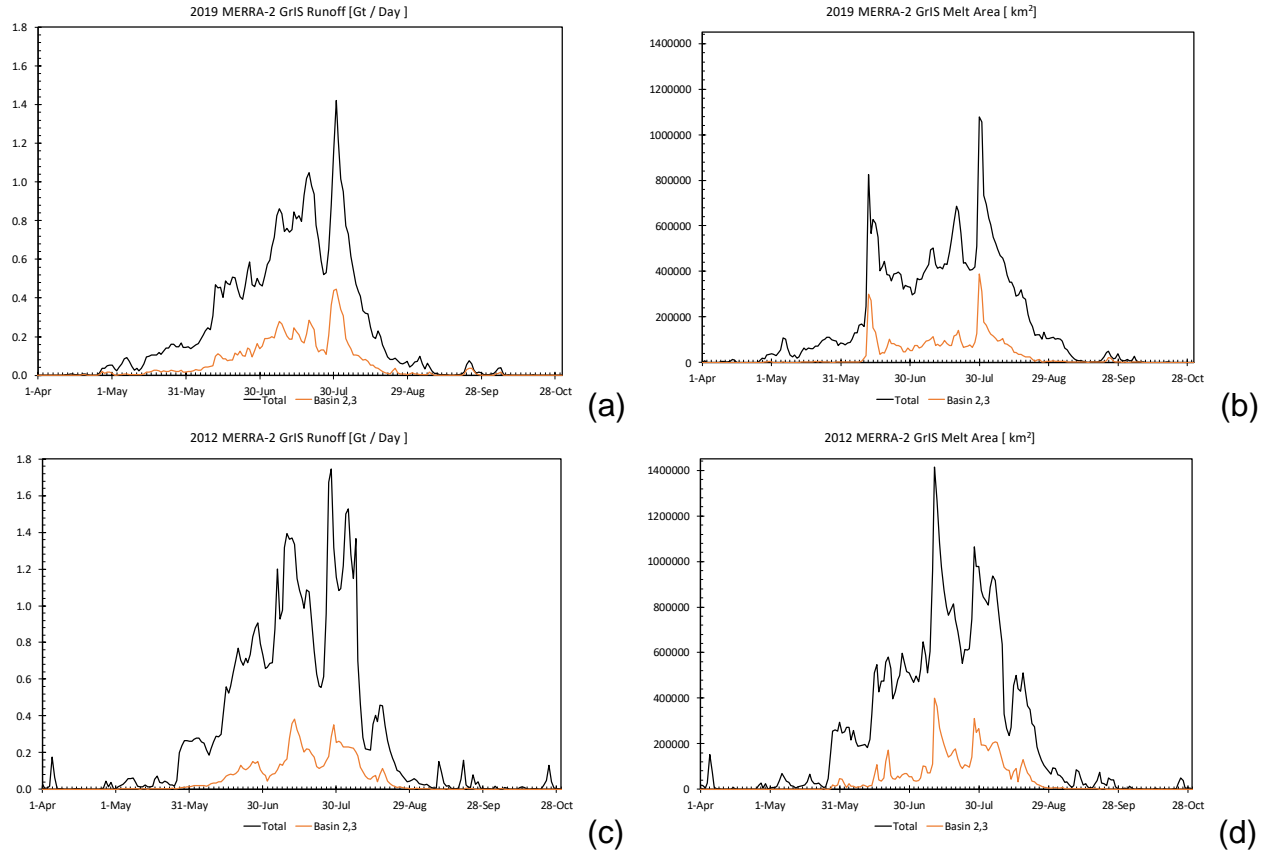


**Figure S6.** Time series of daily GrIS runoff ( $\text{Gt day}^{-1}$ ) and melt area ( $\text{km}^2$ ) from MERRA-2 for the summed drainage basins 2 and 3, and for the full ice sheet for the years (a, b) 2019 and (c, d) 2012. The melt season (April - October) is plotted.

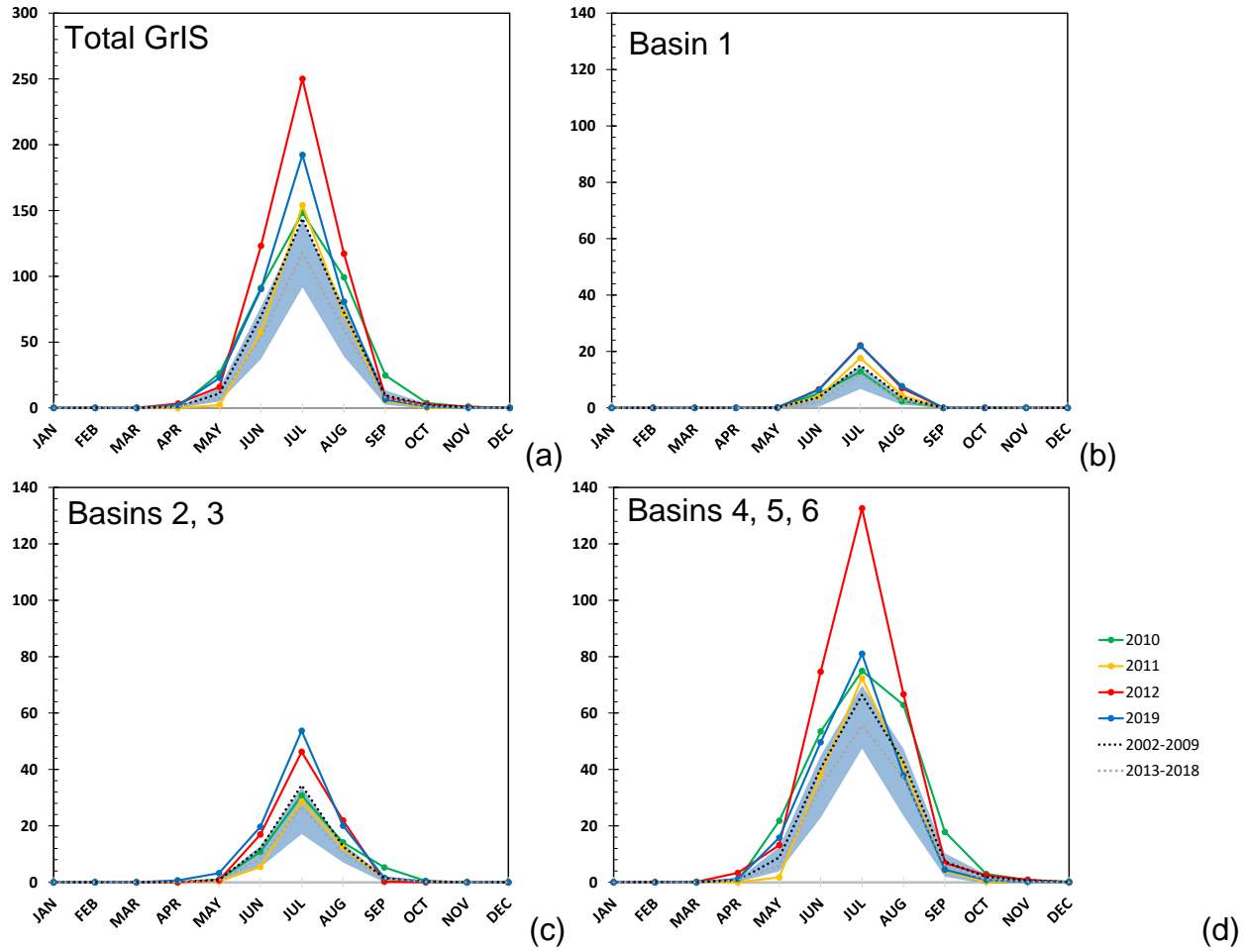


**Figure S7.** Time series of monthly GrIS runoff from MERRA-2 for (a) total GrIS, (b) northern GrIS (Zwally basin 1), (c) eastern GrIS (Zwally basins 2 and 3), and (d) southern GrIS (Zwally basins 4, 5, and 6), in Gt.

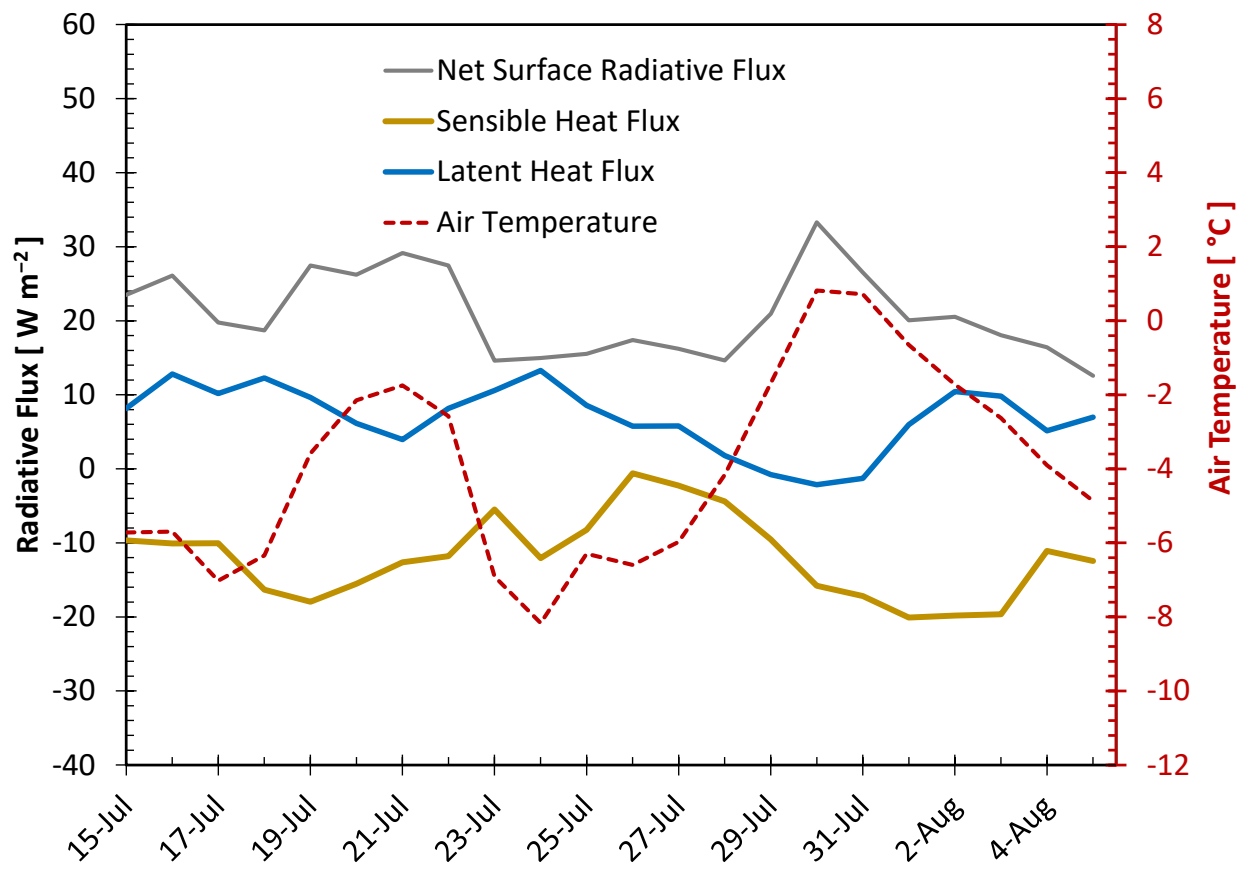


**Figure S8.** Daily surface turbulent and radiative energy budget components from MERRA-2 averaged over basin 3. Flux values are shown in  $\text{W m}^{-2}$ , and surface air temperature is plotted in  $^{\circ}\text{C}$ .

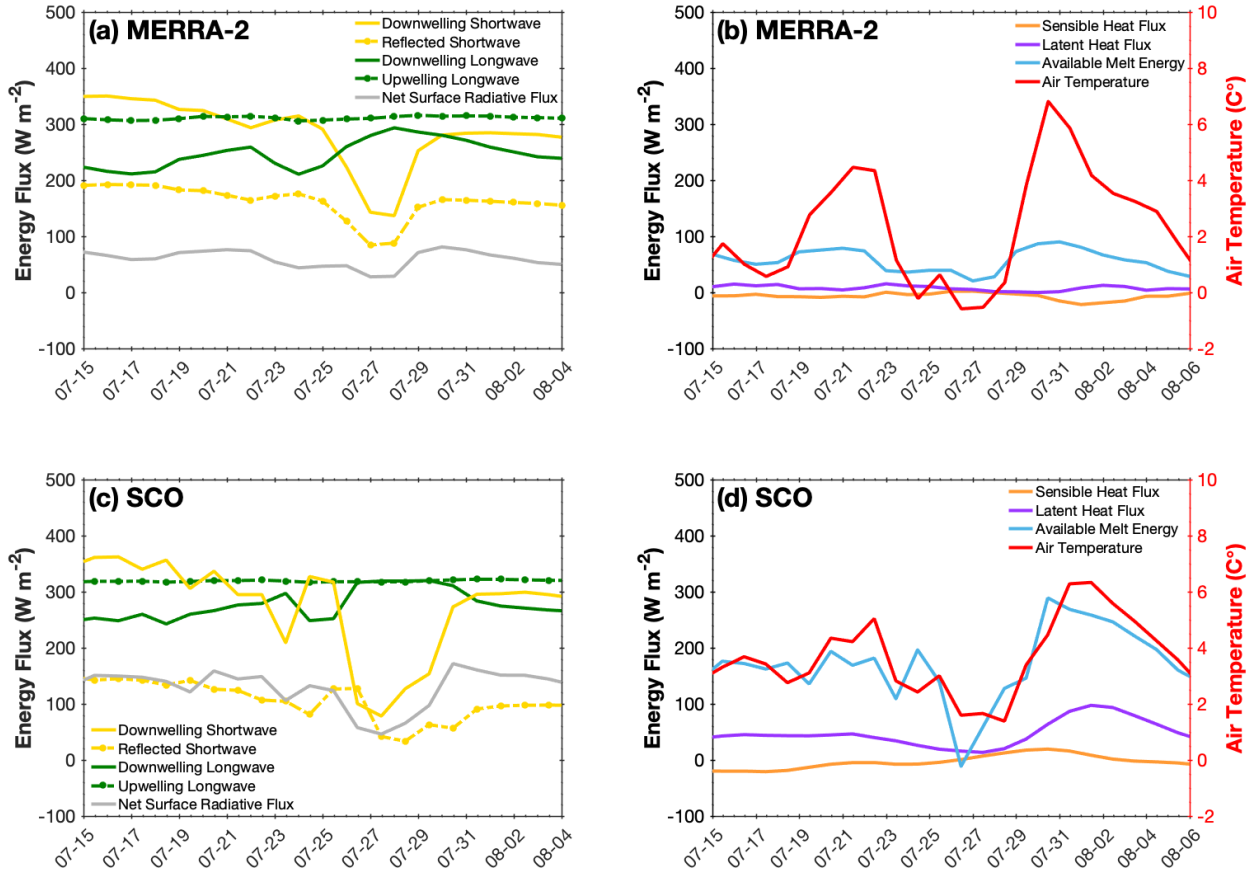


**Figure S9.** Daily-averaged surface radiative energy budget components from MERRA-2 (a) radiative and (b) turbulent flux components, and PROMICE AWS station SCO-U ( $72^{\circ}\text{N}, 27^{\circ}\text{W}, 970\text{ m}$ ) (c) radiative and (d) turbulent flux components. MERRA-2 values correspond to the location of the station. PROMICE turbulent fluxes are averaged from 4-times daily reports. Flux values are plotted in  $\text{W m}^{-2}$ , and surface air temperature is plotted in  $^{\circ}\text{C}$ .

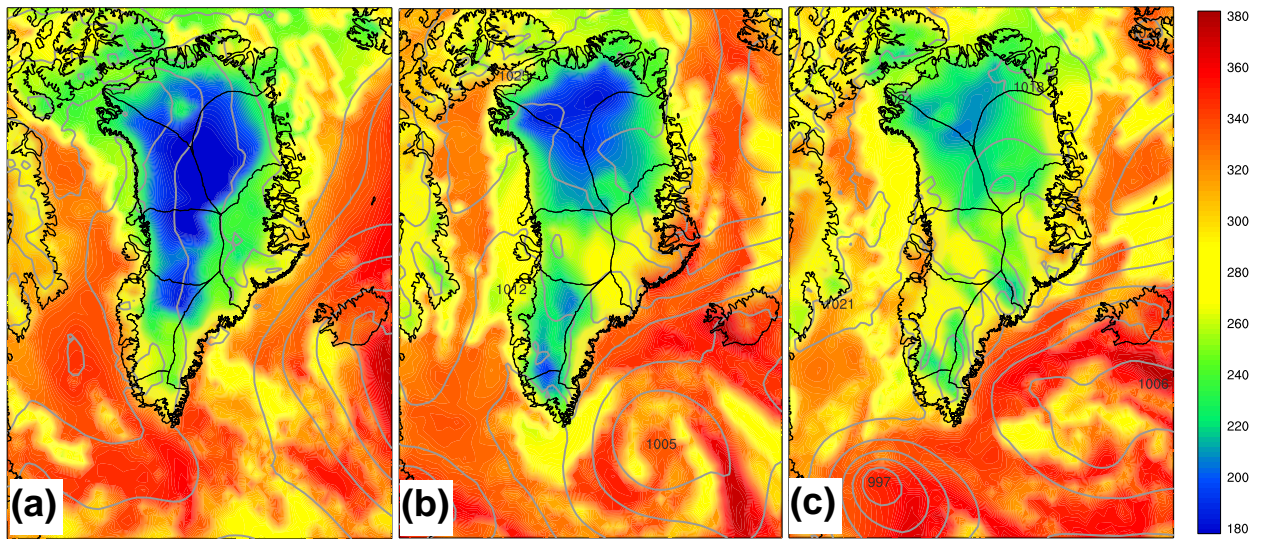


**Figure S10.** MERRA-2 downwelling surface longwave radiative flux for 15Z on (a) 26-July, (b) 29-July, and (c) 30-July, shaded every 5 W m<sup>-2</sup>. Sea level pressure is contoured every 4 hPa, with local maxima indicated.

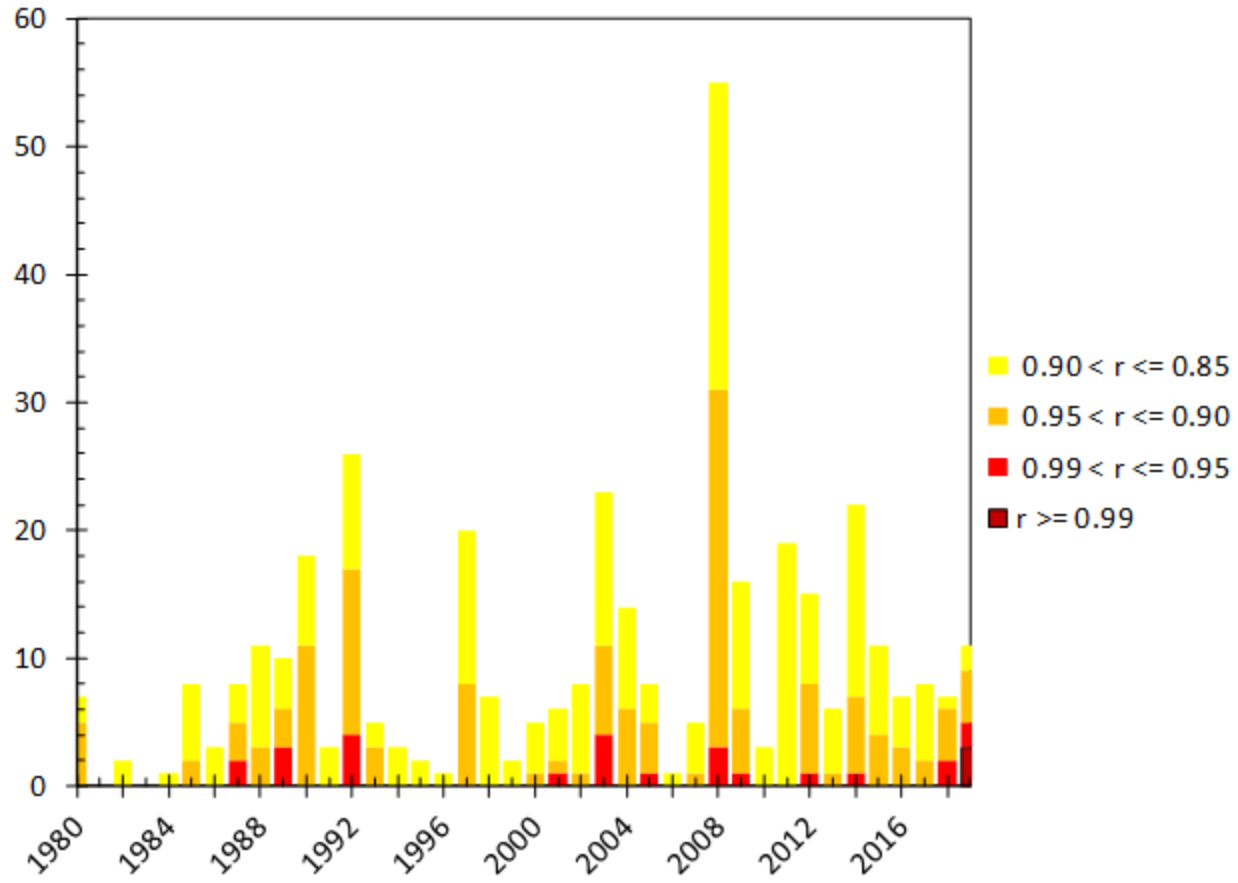


**Figure S11.** Number of occurrences wherein the pattern correlation for the 250 hPa stream function over the boxed area shown in Fig. 1 is within indicated ranges during summer months June, July, and August (JJA). Reanalysis fields are sampled 6-hourly, for a total 368 JJA synoptic times per year.